MICROELECTRONICS RELIABILITY

ELSEVIER

Microelectronics Reliability 44 (2004) 917–928

www.elsevier.com/locate/microrel

Analysis of the reservoir effect on electromigration reliability

Insu Jeon [a,*], Young-Bae Park [b]

[a] PKG & Module R&D Center, Hynix Semiconductor Inc., San 136-1, Ami-ri, Bubal-eub, Ichon-si, Kyoungki-do 467-791, South Korea

[b] Department of Advanced Materials Engineering, Andong National University, Andong City, GyungBuk 760-749, South Korea

Received 25 August 2003; received in revised form 3 February 2004
Available online 15 April 2004

Abstract

The reservoir effect on electromigration reliability is analyzed using the normalized vacancy concentration distribution in the reservoir region of multi-level Al–0.5%Cu interconnect structure. With the assumption of steady state for the vacancy concentration and the fact that no current flow conducts in the reservoir region during electromigration test, a simple equation for calculation of the vacancy concentration is induced. Then direct calculation of the equation is carried out utilizing the hydrostatic stress distribution computed from finite element method to estimate the probability of initial void formation in the reservoir region. Finally, three multi-level Al–0.5%Cu interconnect structures with different reservoir lengths are constructed and electromigration lifetime for the structures is measured to clarify these computational results. From the results of this study, we conclude that the normalized vacancy concentration under the assumption of steady state can be regarded as a quantitative parameter to analyze the reservoir effect on electromigration reliability.
© 2004 Elsevier Ltd. All rights reserved.

1. Introduction

The reservoir is a protrusion of multi-level Al–0.5%Cu interconnects around W via (see Fig. 1). Even though the reservoir does not carry an electric current during electromigration test, the lifetime of the multi-level interconnect systems can be prolonged by the reservoir, which is called 'reservoir effect'. Many experimental works [1–5] for verifying the reservoir effect have been published and all of them demonstrate that electromigration lifetime is dominated by the reservoir area and the number of contacts/vias.

Some numerical works [6–9] for analysis of the reservoir effect by finite element method are also reported. The median-time-to-failure (MTF) calculated by relative resistance change is compared with experimentally measured MTF results of various test structures to show the relation between reservoirs/vias layout and electromigration lifetime. Moreover, to explain the mechanism of void formation around contact/via after electromigration failure, the stress field and its concentration around the area calculated by finite element method are often considered as the quantifying parameter [10–13].

Although these numerical results have a good agreement with the experimental ones, we believe that the stress concentration is insufficient to explain the depletion of Al atoms after electromigration failure in the reservoir region because the stress concentration is related to the cleavage of material junction or the expansion of fractured region around contact/via.

In this paper, three types of multi-level interconnect structures confined by a passivation dielectric, i.e., high density plasma fluorinated silicate glass (HDP FSG), are considered to analyze the reservoir effect on electromigration lifetime, which have different reservoir lengths (R/L) of 0.04, 0.12 and 0.3 μm, and low current density of

* Corresponding author. Present address: Department of Mechanical and Control Engineering, Tokyo Institute of Technology, 2-12-1 O-okayama, Meguro-ku, Tokyo 152-8552, Japan. Tel.: +81-3-5734-2783; fax: +81-3-5734-3917.
E-mail address: i_jeon@mep.titech.ac.jp (I. Jeon).

0026-2714/$ - see front matter © 2004 Elsevier Ltd. All rights reserved.
doi:10.1016/j.microrel.2004.02.001

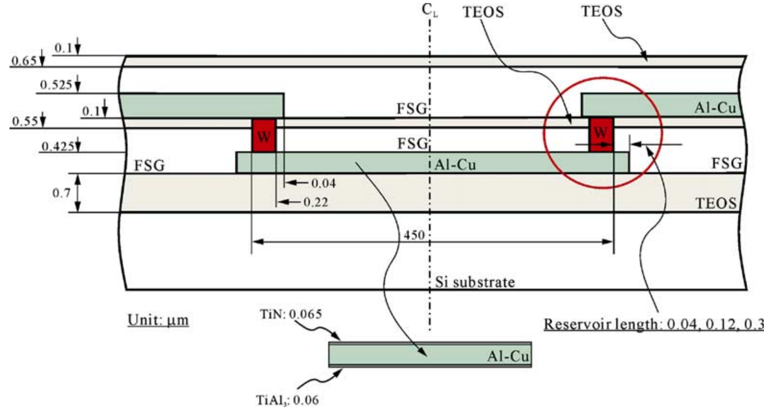

Fig. 1. The multi-level Al–0.5%Cu interconnect structure.

2 MA/cm^2, which is calculated from the cross-sectional area of the Al–Cu interconnect during electromigration test. Because the excessive value of the vacancy concentration is the main cause of void formation [14–16], the reservoir effect is analyzed using the normalized vacancy concentration distribution in the reservoir region of Al–Cu interconnect. A simple equation for the distribution is induced with the assumption of steady state for the vacancy concentration as well as the fact that no current flow conducts in the reservoir region during electromigration test, and the hydrostatic stress distribution in the region computed from finite element method is utilized. When the construction of the three test structures with different reservoir lengths is completed, electromigration lifetime for the structures are measured and then compared with the computational results.

2. Model formulation

Consider the reservoir region of the multi-level interconnect structure (see Fig. 1) in which the vacancy concentration c satisfies the following diffusion–reaction equation [16–18]:

$$\frac{\partial c}{\partial t} = \nabla \cdot \boldsymbol{q} + G, \tag{1}$$

where $\boldsymbol{q}$ is the vacancy flux but the terms that can be determined by electron charge and the electrostatic potential in $\boldsymbol{q}$ are ignored because no current flow conducts in the reservoir region. The reaction rate, G, in this equation models generation and annihilation processes of the vacancy, which can be written as [16–18]

$$G = L_v kT \ln \frac{c}{c_e}, \tag{2}$$

where L_v is a rate parameter, k is Boltzmann's constant, T is the temperature in Kelvin and c_e is the equilibrium vacancy concentration.

Moreover, the stress evolution due to the elastic deformation of the multi-level interconnect system and the vacancy migration as well as generation during electromigration test is given by [17,18]

$$\sigma_{ij} = -B\varepsilon^{v}_{kk}\delta_{ij} + \lambda\varepsilon_{kk}\delta_{ij} + 2\mu\varepsilon_{ij}, \tag{3}$$

where λ and μ are Lame's constants, $B = (3\lambda + 2\mu)/3$ is the bulk modulus, δ_{ij} is Kronecker delta, ε_{ij} is the elastic strain and ε^{v}_{kk} is the strain due to the vacancy migration and generation which can be determined by the rate formation written as

$$\frac{\partial \varepsilon^{v}_{kk}}{\partial t} = \Omega(f\nabla \cdot \boldsymbol{q} + f'G). \tag{4}$$

Here Ω is the volume per Al atom and f is the average vacancy relaxation factor. For Eq. (4), $\varepsilon^{v}_{kk} = 0$ when the vacancy concentration is at stress free state, namely, at $t = 0$ is adopted to prevent the superimposition of the thermal and other stresses on the electromigration induced stress.

Because the reservoir region does not carry an electric current during electromigration test, it is assumed that the vacancy generation and annihilation does not occur in the region. In addition, for the simplicity of the model definition, we consider the steady state for the vacancy concentration. Then the reaction rate, G in Eqs. (2) and (4), and the left term in Eq. (1) go to vanish. Therefore Eqs. (1), (2) and (4) can be replaced by

$$\nabla \cdot \boldsymbol{q} = 0, \tag{5}$$

$$L_v kT \ln \frac{c}{c_e} = 0, \tag{6}$$

$$\frac{\partial \varepsilon^{v}_{kk}}{\partial t} = 0. \tag{7}$$

Here, it is found that Eq. (7) means $\varepsilon^{v}_{kk} = 0$ everywhere at all times $t > 0$ because of the assumption for Eq. (4) that is $\varepsilon^{v}_{kk} = 0$ everywhere at $t = 0$.

The equations above show two important facts of the electromigration problem: Firstly, under the consideration of the steady state for the vacancy concentration, there is no stress evolution in Eq. (3) caused by the vacancy migration and generation in the reservoir region. Secondly, the vacancy concentration can be easily determined through Eq. (6), i.e., $c = c_e$, without solving Eq. (1). The well-known equation of the equilibrium vacancy concentration in the presence of mechanical stress has the form [19–22]

$$c_e = c_0 \exp(f'\Omega\sigma/kT), \qquad (8)$$

where c_0 is the equilibrium concentration in the absence of stress, $f' = 1 - f$ and σ is the hydrostatic stress.

Therefore, the vacancy concentration distribution may be easily calculated using Eq. (8) with the hydrostatic stress field in the reservoir region. The calculated vacancy concentration makes it possible to estimate the probability of initial void formation in the reservoir region. The numerical calculation process of the hydrostatic stress is introduced in the next section.

3. Computational approach

For numerical calculation of the hydrostatic stress in the reservoir region, finite element meshes for multi-level Al–0.5%Cu interconnect structure shown in Fig. 1 are constructed. Due to the symmetry of the structure, only the right half of the structure is considered. Also, for the sake of simplicity in numerical analysis, a small part around the reservoir region in the right half of the structure is modeled as long as the effect of the boundary on the stress field in the reservoir region is small, which is shown in Fig. 2. Therefore, for the boundary conditions of this model, the symmetric condition is applied on the left edge and *x*- and *y*-direction constraints are loaded on the right and the bottom edge, respectively. The three different reservoir lengths in Metal 1 are considered as 0.04, 0.12 and 0.3 μm while the reservoir length of Metal 2 is fixed as 0.04 μm (see Figs. 2 and 3). For more accurate calculation of the stress field, very fine element structure is constructed around the edge of the reservoir, which is shown in Fig. 3(a).

The package code ABAQUS is employed for finite element solution and the isoparametric plane strain elements with eight nodes are used to calculate the stress field in the structures under the assumption of a good adhesion between dissimilar materials and a uniform temperature at each temperature step. In addition, stress-free state of the model is assumed at inter-level dielectric (ILD) deposition temperature, 400 °C. The intrinsic stress of each constituent material is ignored based on the assumption that it can be fully relaxed during ILD deposition process, which is revealed in some earlier works [11–13]. Therefore, the stress calculated in this study is the thermal stress that stems from the mismatch of material properties between dissimilar materials.

Table 1 summarizes the material properties used in this analysis where each value of Young's modulus at room temperature is measured by nanoindentation method [23]. For the mechanical property data of thin (∼60 nm) $TiAl_3$ layer formed under Al–Cu metal line (see Figs. 1 and 2), however, measured Young's modulus of Ti is used in finite element analysis because of the difficulty of experiment. Particularly, the temperature-dependent material properties are used for Al–Cu metal line [24–26]. For more practical situation during

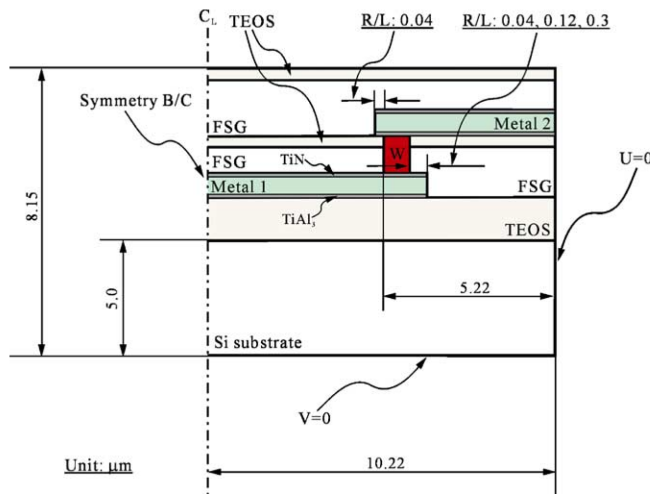

Fig. 2. The modeled small region around the reservoir for the numerical calculation.

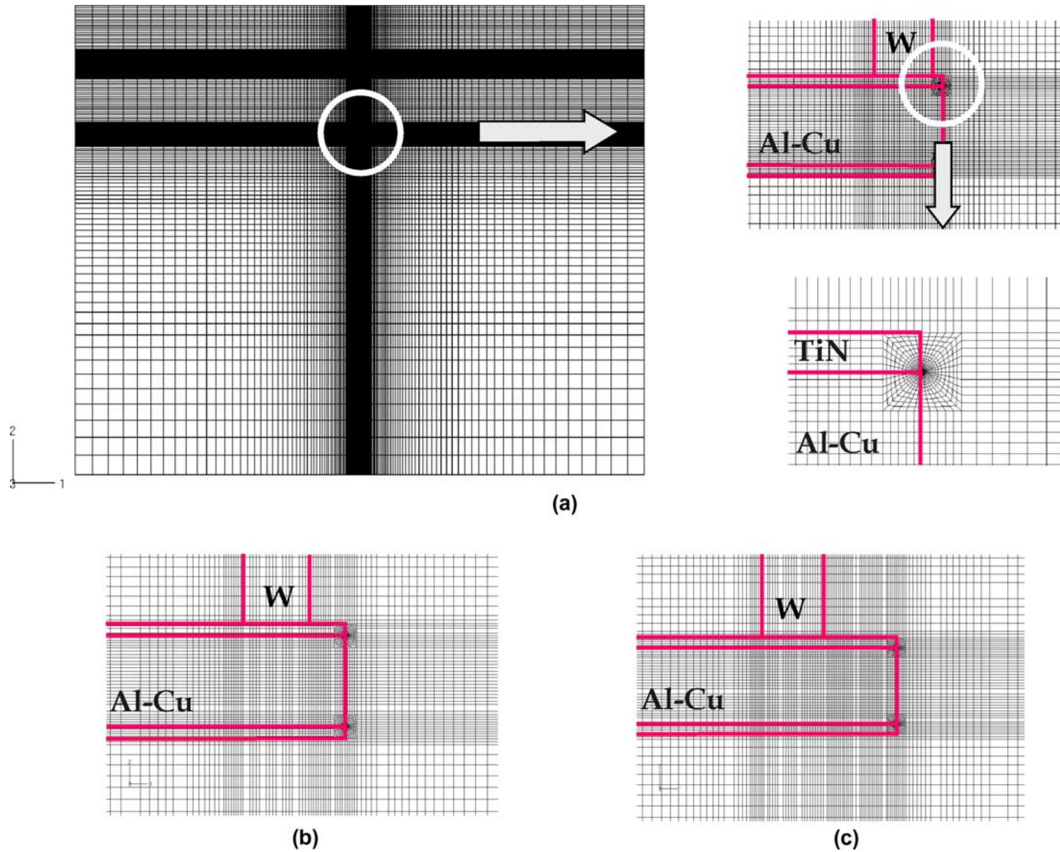

Fig. 3. The finite element mesh for the modeled region: (a) $R/L = 0.04$ μm, (b) $R/L = 0.12$ μm, and (c) $R/L = 0.3$ μm.

Table 1
The material properties for the numerical calculation

	E^a (GPa)	v	CTE (ppm/K)	Yield stress (MPa)
Si	145	0.26	2.6	
Al–Cu	59−0.04(T-20)	0.34	24.3 + 0.02(T-20)	200−0.35(T-20)
FSG	51	0.19	3	
FOX	8	0.19	20.5	
PETEOS	75	0.24	1	
TIN	270	0.25	9.4	
Ti($TiAl_3$)	140	0.25	8.9	
W	411	0.28	4.5	

[a] Measured by nanoindentation method.

fabrication and electromigration test, it is assumed that Al–Cu metal line follows the Prandtl–Reuss equations for the incremental plasticity theory of the isotropic-hardening materials and the calculation of the equation is processed with a power-law hardening rule of the form [27,28]

$$\frac{\bar{\varepsilon}^{p}}{\varepsilon_{Y}} = \alpha\left(\frac{\bar{\sigma}}{\sigma_{Y}}\right)^{m}. \quad (9)$$

Here σ_Y is the uniaxial yield stress, $\bar{\varepsilon}^p$ is the plastic equivalent strain, and $\varepsilon_Y = \sigma_Y/E$ is a reference strain component, $\bar{\sigma}$ is the Mises stress, α is a non-dimensional material constant and m is the power-law hardening exponent. For the numerical computation, $\alpha = 1$ and $m = 12$ are chosen and the reduced integration element is selected to prevent the excessive incompressibility constraint due to plastic deformation.

The temperature boundary condition as an external load for this numerical calculation is decided by cooling

the model from ILD deposition temperature, 400 °C to room temperature, 20 °C and then by heating to electromigration test temperature, 200 °C. The stress distribution is then calculated from the electromigration test state.

4. Results and discussion

Generally, three types of failure are found in multi-level interconnects during electromigration test as shown in Fig. 4. The failure shape in Fig. 4(a) is mainly affected by the current density and the one shown in Fig. 4(c) is affected by the condition of barrier metal layered on the Metal 1. However, because the low current density, 2 MA/cm^2, calculated during this electromigration test and TiN layer under W via of this study can be robust 'blocking boundary' for Al atoms migration [29–31], we only focus on the second type of failure to analyze the reservoir effect on electromigration lifetime shown in Fig. 4(b).

Before calculating the vacancy concentration in the reservoir region, the hydrostatic stress field of the multi-level interconnect structure is computed using finite element method because the hydrostatic stress is the only stress parameter to determine the vacancy concentration in Eq. (8). From the computed results of the hydrostatic stress in whole structures, the stress distributions in the three different reservoir regions are used to calculate the vacancy concentration distributions, which are presented in Fig. 5. In this figure, *x*- and *y*-coordinate of the reservoir region are normalized by the maximum R/L of this study, 0.3 μm and the thickness of Metal 2, 0.3 μm, respectively. The positive singular hydrostatic stresses

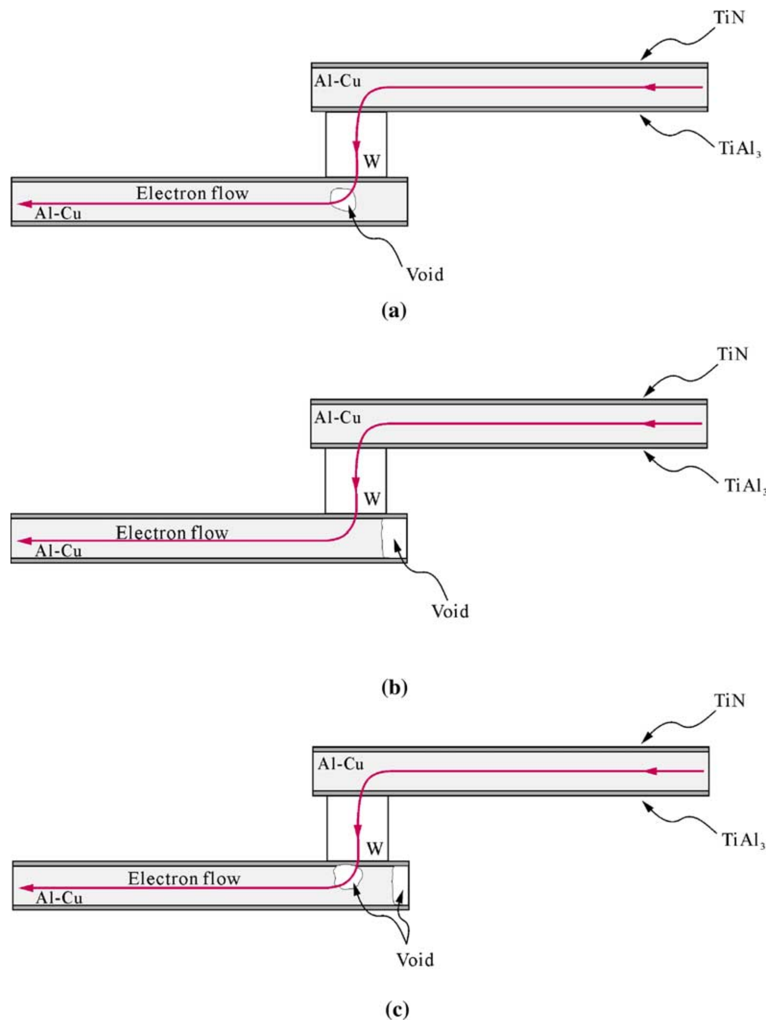

Fig. 4. Three types of electromigration failure in multi-level metal interconnects.

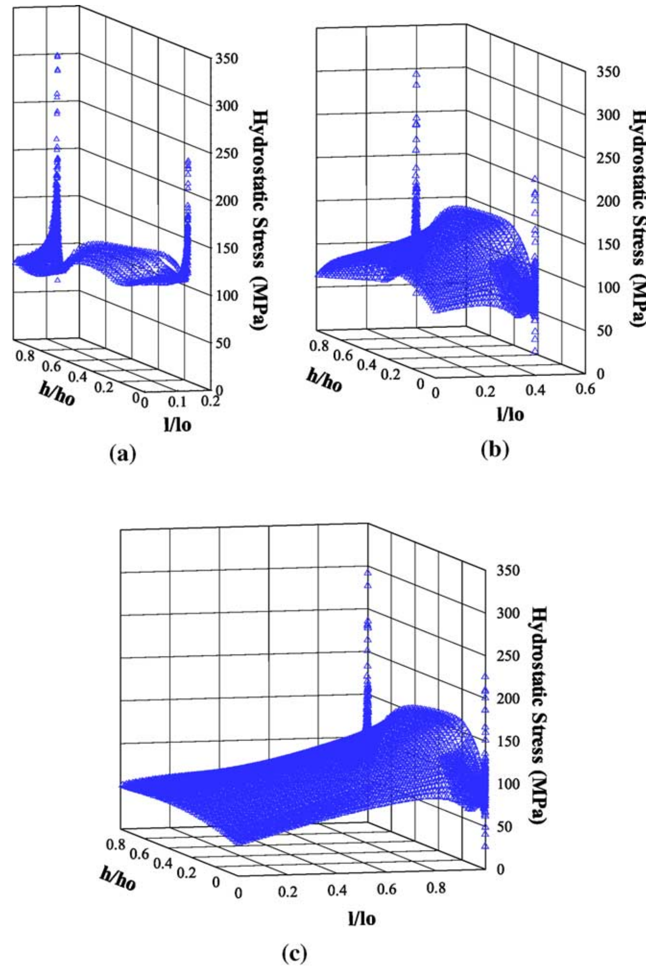

Fig. 5. The hydrostatic stress distribution in the reservoir regions: (a) $R/L = 0.04$ μm, (b) $R/L = 0.12$ μm, and (c) $R/L = 0.3$ μm.

are found around the upper and the lower edge of the reservoir. These stress concentrations result from the stress singularities around the triple junction vertex of the edges that can be determined by the near field condition, i.e., the continuity condition of traction and displacement in the interface of each material.

The vacancy concentration distribution in the reservoir region, therefore, can be easily calculated using Eq. (8) with the hydrostatic stress field in Fig. 5 and the constant parameters presented in Table 2. The calculated vacancy concentration distribution that is normalized by c_0 is shown in Fig. 6. It is notable that the negative singular stress and the non-singular stress have no or less effect on the vacancy concentration due to the exponential characteristics of $c_e = c$ in Eq. (8). Thus the excessive vacancy concentration is calculated around the upper and the lower edge of the reservoir due to the calculated positive singular stress. These results suggest that the probability of void formation is extremely high in these sites.

Table 2
The parameters used to calculate the vacancy concentration distribution

c_0	Average vacancy concentration	1.37×10^{19}/cm^3
f	Average vacancy relaxation factor [16]	0.2
Ω	Volume per Al atom, bulk	1.68×10^{-23} cm^3
k	Boltzmann's constant	8.62×10^{-5} eV/K

Fig. 7 shows the maximum normalized vacancy concentration of each R/L. The small decrease but almost same values of maximum normalized vacancy concentration along with the change of R/L from 0.04 to 0.3 μm is found in this figure. It means that the probability of void formation does not change significantly with increase of the reservoir length. In this case, therefore, more longer electromigration lifetime of the structures with $R/L = 0.3$ μm than that of the structure with $R/L = 0.04$, 0.12 μm can be estimated. Because the

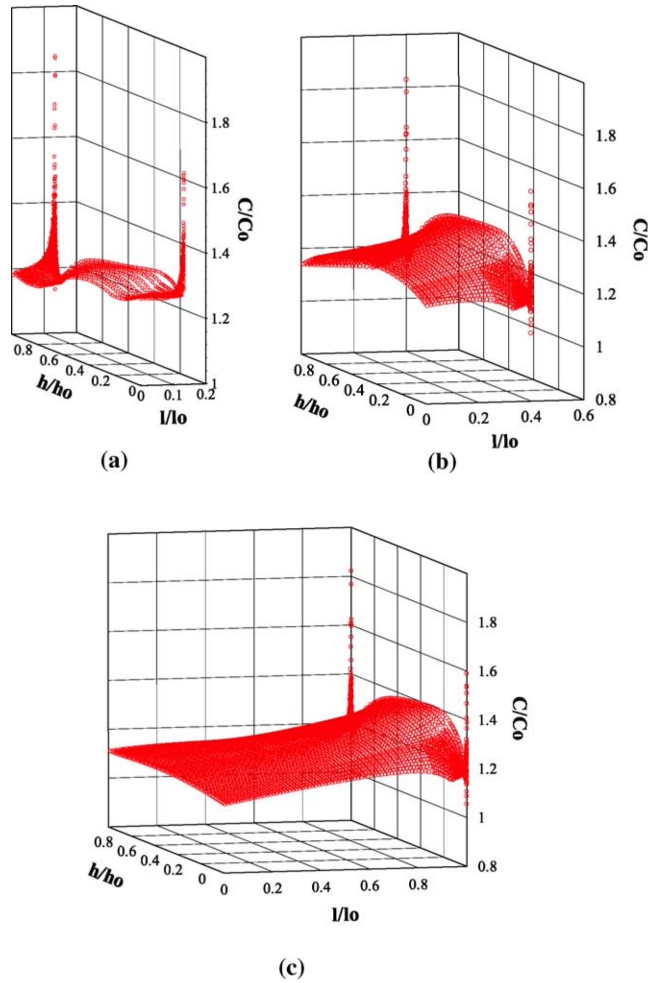

Fig. 6. The vacancy concentration distribution in the reservoir regions: (a) $R/L = 0.04$ μm, (b) $R/L = 0.12$ μm, and (c) $R/L = 0.3$ μm.

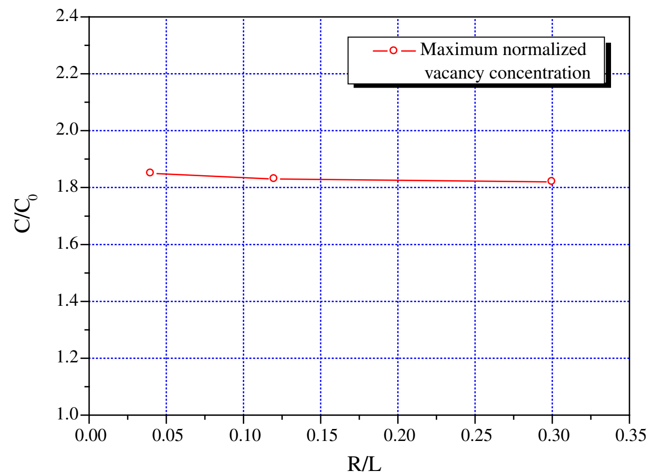

Fig. 7. The change of the maximum normalized vacancy concentration in the reservoir region with the change of the reservoir length.

metal reservoir area provides Al and/or Cu atoms that diffuse and replaces those atoms that have been removed near the W via, at least until the atoms in the reservoir are depleted [2]. Therefore, we can explain the reservoir effect on the electromigration lifetime with these calculated results, even though we do not know the critical value of vacancy concentration on the Al–Cu metal line.

Particularly, for a numerical example, FSG is replaced by flowable oxide (FOX), which is often used as a passivation material for the multi-level interconnect structure, and the same calculation process for the vacancy concentration is carried out. The normalized vacancy concentration distribution calculated in the reservoir region ($R/L = 0.12$ μm) is presented in Fig. 8. The circled region in Fig. 8 clearly shows that the normalized vacancy concentration has been decreased in this example. Fig. 8, therefore, illustrates that the excessive vacancy concentration around the edge of the reservoir is not the general phenomenon of the multi-level interconnect structures.

The three types of the test structure with two-level metallization are fabricated using P-type ⟨1 0 0⟩ Si wafer and electromigration lifetime of these structures is measured to clarify the computational results. At first, plasma enhanced chemical vapor deposited (PECVD) oxide of 700 nm is prepared on the wafer. A bottom–Ti(10 nm)\Al–0.5%Cu(350 nm)\Ti(5 nm)\TiN(60 nm)–top stack is then deposited using a multi-chamber dc magnetron sputtering system without vacuum break. That is, 10 nm of Ti is deposited, which is followed by in situ sputter deposition of 350 nm of Al–0.5%Cu with process power of 12 kW at 400 °C. On the top of Ti\Al structure, 5 nm of Ti and 60 nm of TiN are deposited in a single chamber.

The metal stack is patterned by the standard photolithography and the plasma dry etching. Then, FSG is deposited on the patterned metal lines. This is followed by deposition of plasma enhanced tetra ethyl ortho silicate (PETEOS) film and subsequent planarization by chemical–mechanical polishing (CMP), which results in ILD of FSG\PETEOS. After via hole opening and Ar sputter etching are carried out, via plugs are fabricated by in situ deposition of Ti\TiN liner, CVD W deposition, and W CMP. The same processes are repeated to make the second level structure and finally pad for wire bonding to package is opened by patterning process.

A cross-sectional transmission electron microscope (TEM) photograph around W via of electromigration test structure is shown in Fig. 9. It is found that Ti–Al reaction layer ($TiAl_3$, ~60 nm) is formed uniformly across the bottom–Ti\Al interface while no reaction was observed at Al\top–Ti(slightly nitrized) interface. The

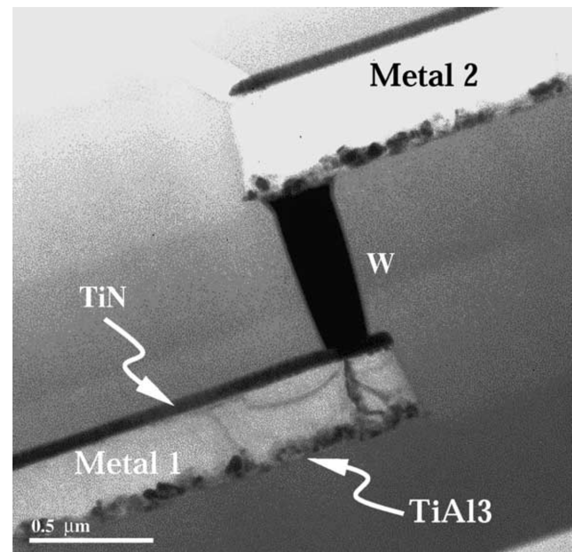

Fig. 9. The cross-sectional TEM photograph around W via of the test structure.

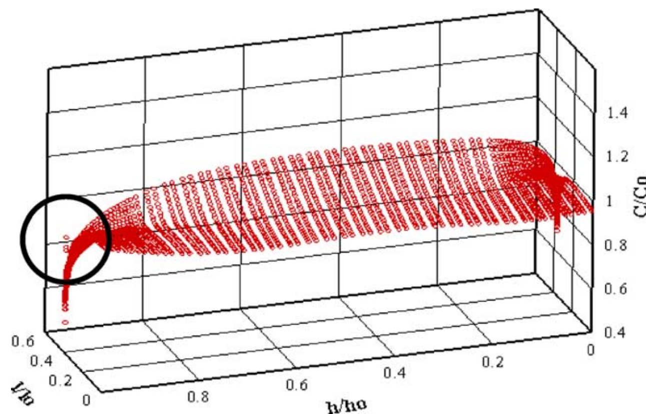

Fig. 8. The calculated vacancy concentration distribution using flowable oxide (FOX) instead of FSG ($R/L = 0.12$ μm).

lower metal line, Metal 1, layer is 0.2 μm wide, 0.425 μm thick and 450 μm long straight line. The upper metal line, Metal 2, layer is 0.24 μm wide, 0.425 μm thick and 50 μm long straight line connected with the bonding pad for the chip packaging. The wafers are annealed for 50 min at 400 °C in a forming gas (N_2/H_2) ambient for stabilization of microstructure before an accelerated electromigration testing. In package-level electromigration test, ambient temperature and current density are 200 °C and 2 MA/cm^2, respectively.

Fig. 10 shows the cumulative percentage of the time to failure for both 3% and 20% failure criterion, which means the electromigration lifetime when the resistance increases 3% and 20%, respectively. The 3% failure criterion means the initial void formation around the reservoir edges and the 20% failure criterion represents the depletion of Al and Cu atoms in the reservoir. The results of electromigration test in Fig. 10 are summarized in Table 3. The measured joule-heating temperatures are under 5 °C, which is ignorable temperature condition to analyze the electromigration reliability at 200 °C. Median time to failure (MTTF) is obtained from a best-fit straight line drawn through data points in the log–normal plot of time to failure as shown in Fig. 10, which is given by the intercept at the 50% cumulative failure point (t_{50}) [29,30]. Table 3 clearly shows that electromigration lifetime is improved much better for the metal

Table 3
The measured electromigration lifetimes of the three test structures

Reservoir length (μm)	Electromigration lifetime (MTTF)	
	3% Failure criteria [h]	20% Failure criteria [h]
0.04	30.8	48.0
0.12	31.9	52.3
0.30	113.5	126.3

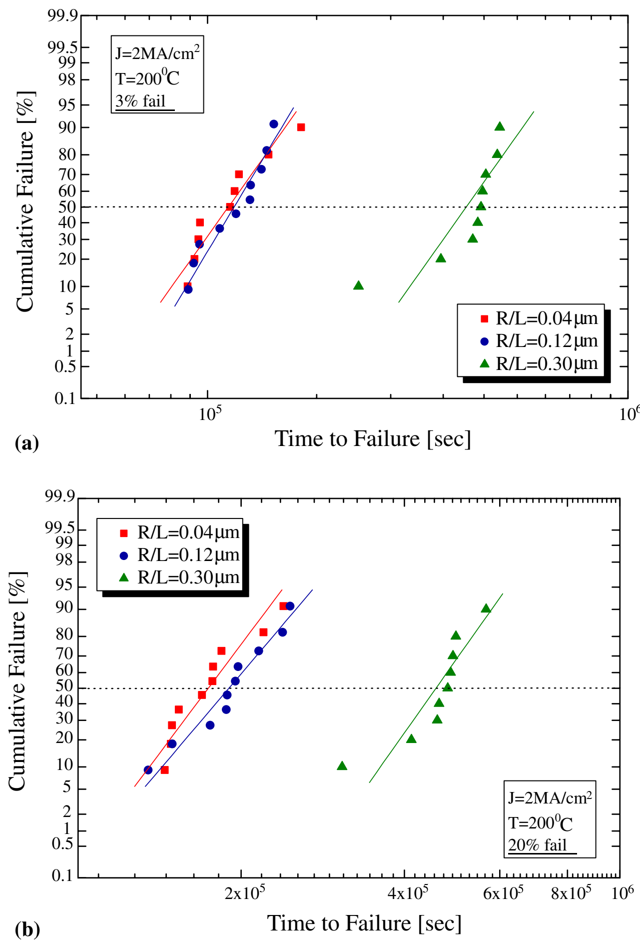

Fig. 10. The cumulative percentage of the time to failure for (a) 3% failure criterion (b) 20% failure criterion.

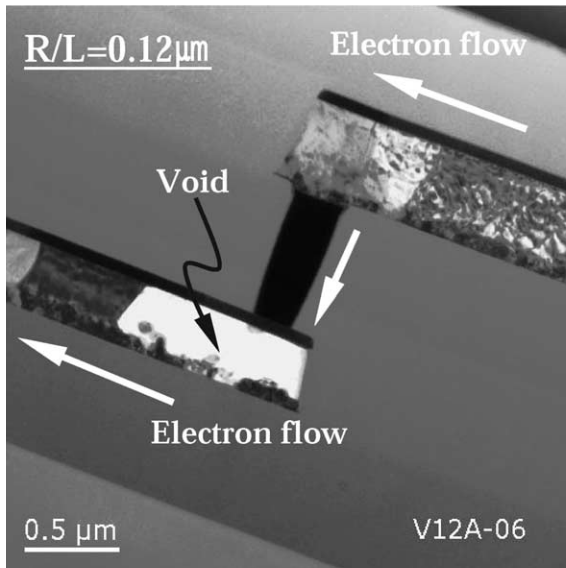

Fig. 11. The cross-sectional TEM image after the resistance increases 20%.

interconnection with larger reservoir (0.3 μm) in both case of 3% and 20% criteria. The dependence of electromigration lifetime on the reservoir length for smaller size ranges (0.04 and 0.12 μm) is also certain for both criteria.

Because the normalized vacancy concentration shows the probability of the initial void formation in the reservoir, the trend of these calculated results can be compared with the experimental ones of the 3% failure criterion and it is found that these results have a good agreement with the experimental ones. Also, the little difference in lifetime trend of the experimental results between 3% and 20% failure criterion means that the calculated normalized vacancy concentration can be a good parameter to analyze the reservoir effect on the electromigration reliability. One of the failed specimens that is analyzed by cross-sectional TEM after the resistance increases 20% is presented in Fig. 11 and it shows the second electromigration failure type of Fig. 4(b).

The limitation of this research, however, is the fact that the steady state of the vacancy concentration is assumed to analyze the reservoir effect. The vacancy concentration in the region A of Fig. 12 will depend on the time during the electromigration test due to the current flow. Thus the vacancy concentration of the reservoir region also depends on time because of the material continuity. Considering the transient behavior of the vacancy concentration, therefore, is more realistic to analyze the reservoir effect. The difference, however, between the results obtained under these two assumptions of the steady state and the transient state can be simply explained using the region B in Fig. 12.

In the region A of Fig. 12, the vacancy concentration will be generated and annihilated and also the stress field will be changed due to the electron flow. These changed values will replace the boundary condition on the left side of the region B in Fig. 12, which can change the whole state of the vacancy concentration in the reservoir region during electromigration test. Actually, the role of the changed vacancy concentration distribution on the left boundary is the vacancy supply from the region A to

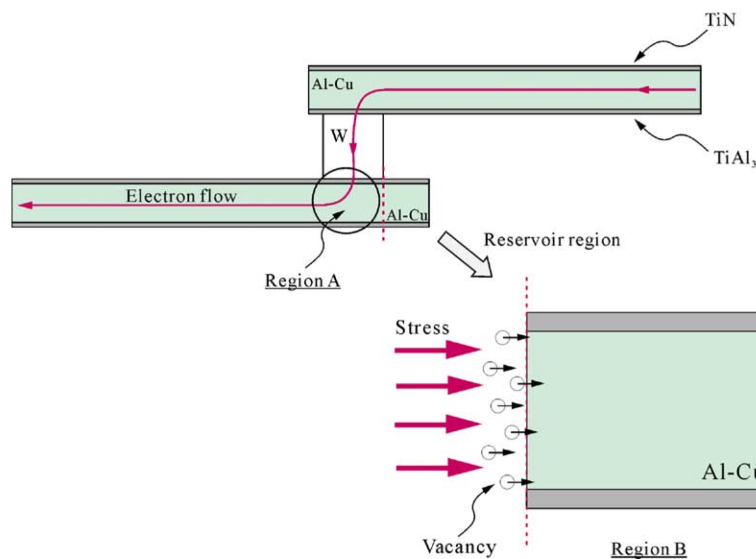

Fig. 12. The effect of the transient state of the vacancy concentration on the reservoir region during the electromigration test.

the region B (see Fig. 12). Then it will increase the vacancy concentration level in the reservoir region during the electromigration test. Moreover, the changed stress field on the left boundary can change the stress distribution or the stress gradient in the reservoir region.

However, consider the stress field and the strain rate in Eqs. (3) and (4). It is shown that the stress field connected with the vacancy migration and generation can be determined by ∇q and G, which are components of Eq. (1). Therefore, if there is no geometric singularity, for example, the dislocation or the material defect around the left boundary of the reservoir, the stress fields on the left boundary still maintain non-singular during the electromigration test. This means that the trend of the stress distribution and the vacancy concentration distribution in the reservoir region still do not change during the test but the magnitude of these values will increase due to not only the evolved stress but also the vacancy supply from the left boundary. Therefore, the normalized vacancy distribution under the assumption of steady state has a reasonable meaning to estimate initiation of the void formation and also the electromigration reliability of the metal interconnect structure. In addition, the computational analysis in this study can give a lot of advantages because of its simplicity and efficiency in calculation of the vacancy concentration that can be used for design of the reliable metal systems comparing with various shapes of reservoir.

5. Conclusion

For analyzing the reservoir effect, calculation of the vacancy concentration in the reservoir region is carried out. The thermal stresses of the three multi-level interconnect structures are computed using finite element method. Moreover, three different types of the test structure are constructed and electromigration lifetime of these test structures are measured to clarify the results of computational analysis.

From the results of this study, we conclude that the normalized vacancy concentration under the assumption of steady state can be regarded as a quantitative parameter to analyze the reservoir effect on electromigration reliability. Furthermore, it can be easily used to design the reliable metal systems with reservoir for actual FAB process due to its simplicity and efficiency for calculation.

References

[1] Le HA, Ting L, Tso NC, Kim CU. Analysis of the reservoir length and its effect on electromigration lifetime. J Mater Res 2002;17:167–71.

[2] Dion MJ. Reservoir modeling for electromigration improvement of metal systems with refractory barriers. In: Proc IEEE Int Reliab Phys Symp, 2001. p. 327–33.

[3] Dion MJ. Electromigration lifetime enhancement for lines with multiple branches. In: Proc IEEE Int Reliab Phys Symp, 2000. p. 324-32.

[4] Skala S, Bothra S. Effects of W-plug via arrangement on electromigration lifetime of wide line interconnects. In: Proc IEEE Int Interconnect Technol Conf, 1998. p. 116–8.

[5] Fujii M, Koyama K, Aoyama J. Reservoir length dependence of EM lifetime for Tungsten via chain under low current stress. In: Proc 13th Int VLSI Multilevel Interconnection Conf, 1996. p. 312–7.

[6] Nguyen HV, Salm C, Wenzel R, Mouthaan AJ, Kuper FG. Simulation and experimental characterization of reservoir and via layout effects on electromigration lifetime. Microelectron Reliab 2002;42:1421–5.

[7] Nguyen HV, Salm C, Wenzel R, Mouthaan AJ, Kuper FG. Modelling of the reservoir effect on electromigration lifetime. In: Proc 8th Int Symposium on the Physical & Failure Analysis of Integrated Circuits, 2001. p. 169–73.

[8] Nguyen HV, Salm C, Kuper FG, Mouthaan AJ. Simulations of reservoir effect in multilevel Al-based metallisation. In: Proc Safe/IEEE Workshop, 2000. p. 101–5.

[9] Petrescu V, Mouthaan AJ, Schoenmaker W, Salm C. Mechanical stress evolution and the Blech length: 2D simulation of early electromigration effects. Microelectron Reliab 1998;38:1047–50.

[10] Shen YL, Guo YL, Minor CA. Voiding induced stress redistribution and its reliability implications in metal interconnects. Acta Mater 2000;48:1667–78.

[11] Shen YL. Stresses, deformation, and void nucleation in locally debonded metal interconnects. J Appl Phys 1998; 84:5525–30.

[12] Shi LT, Tu KN. Finite element stress analysis of failure mechanisms in a multilevel metallization structure. J Appl Phys 1995;77:3037–41.

[13] Shi LT, Tu KN. Finite element modeling of stress distribution and migration in interconnecting studs of a three-dimensional multilevel device structure. Appl Phys Lett 1994;65:1516–8.

[14] Hu CK, Gignac L, Malhotra SG, Rosenberg R. Mechanisms for very long electromigration lifetime in dual-damascene Cu interconnections. Appl Phys Lett 2001; 78:904–6.

[15] Rosenberg R, Ohring M. Void formation and growth during electromigration in thin films. J Appl Phys 1971; 42:5671–9.

[16] Kirchheim R. Stress and electromigration in Al-line of integrated circuits. Acta Metall Mater 1992;40:309–23.

[17] Sarychev ME, Zhitnikov YV, Borucki L, Liu CL, Makhviladze TM. A new, general model for mechanical stress evolution during electromigration. Thin Solid Films 2000; 65:211–8.

[18] Sarychev ME, Zhitnikov YV, Borucki L, Liu CL, Makhviladze TM. General model for mechanical stress evolution during electromigration. J Appl Phys 1999;86:3068–75.

[19] Clement JJ. Reliability analysis for encapsulated interconnect lines under dc and pulsed dc current using a continuum electromigration transport model. J Appl Phys 1997; 82:5991–6000.

[20] Clement JJ, Thompson CV. Modeling electromigration-induced stress evolution in confined metal lines. J Appl Phys 1995;78:900–4.
[21] Korhonen MA, Borgesen P, Tu KN, Li CY. Stress evolution due to electromigration in confined metal lines. J Appl Phys 1993;73:3790–9.
[22] Clement JJ, Lloyd JR. Numerical investigations of the electromigration boundary value problem. J Appl Phys 1992;71:1729–31.
[23] Oliver WC, Pharr GM. An improved technique for determining hardness and elastic modulus using load and displacement sensing indentation experiments. J Mater Res 1992;7:1564–83.
[24] Park YB, Jeon I. Mechanical stress evolution in metal interconnects for various line aspect ratios and passivation dielectrics. Microelectron Eng 2003;69:26–36.
[25] Gouldstone A, Shen YL, Suresh S, Thompson CV. Evolution of stresses in passivated and unpassivated metal interconnects. J Mater Res 1998;13:1956–66.
[26] Sauter AI, Nix WD. Thermal stress in Aluminum lines bonded to substrates. IEEE Trans Comp Hybrids Manufact Technol 1992;15:594–600.
[27] Jeon I, Lee Y, Im S. Higher order eigenfields in mode II cracks under elastic–plastic deformation. KSME Int J 2003;17:254–68.
[28] Jeon I, Im S. The role of higher order eigenfields in elastic–plastic crack. J Mech Phys Solids 2001;49:2789–818.
[29] Estabil JJ, Rathore HS, Levine EN. Electromigration improvements with titanium underlay and overlay in Al(Cu) metallurgy. In: Proc 7th Int IEEE VLSI Multilevel Interconnection Conf, 1991. p. 242–8.
[30] Hosaka M, Kouno T, Hayakawa Y. Ti layer thickness dependence on electromigration performance of Ti/AlCu metallization. In: Proc IEEE Int Reliab Phys Symp, 1998. p. 329–34.
[31] Park YB, Lee DW. Effects of Ti and TiN underlayers on electromigration reliability of Al–Cu interconnects. Mater Sci Eng B 2001;87:70–6.